

# VaLiD: Mitigating the Hallucination of Large Vision Language Models by Visual Layer Fusion Contrastive Decoding

Jiaqi Wang  
Beijing Jiaotong University  
Beijing, China  
jiaqiwbjtu.edu.cn

Yifei Gao  
Beijing Jiaotong University  
Beijing, China  
yifeigao@bjtu.edu.cn

Jitao Sang\*  
Beijing Jiaotong University  
Beijing, China  
jtsang@bjtu.edu.cn

## Abstract

Large Vision-Language Models (LVLMs) have demonstrated outstanding performance in multimodal task reasoning. However, they often generate responses that appear plausible yet do not accurately reflect the visual content, a phenomenon known as hallucination. Recent approaches have introduced training-free methods that mitigate hallucinations by adjusting the decoding strategy during inference stage, typically attributing hallucination to the language model itself. Our analysis, however, reveals that distortions in the visual encoding process significantly affect the model’s reasoning accuracy. Specifically, earlier visual layers may retain key features but gradually distort as the information propagates toward the output layer. Building on these findings, we propose a novel hallucination-mitigation method from the visual encoding perspective: **Visual Layer Fusion Contrastive Decoding (VaLiD)**. This method utilizes uncertainty to guide the selection of visual hidden layers, correcting distortions in the visual encoding process and thereby improving the reliability of generated text. Experimental results show that VaLiD effectively reduces hallucinations across various benchmarks, achieving state-of-the-art performance compared to multiple baseline methods.

## 1. Introduction

Large Vision-Language Models (LVLMs) have demonstrated remarkable capabilities [2, 7, 29] in multi-modal understanding and reasoning tasks, including Visual Question Answering [1, 36], Cross-Modal Retrieval [40], and Visual Reasoning [17], marking them as critical milestones on the path toward Artificial General Intelligence (AGI) [3]. However, despite their impressive performance across various tasks, LVLMs still cannot overcome the issue of hallucination [14, 23]. This problem substantially weakens the reliability of LVLMs, presenting significant obstacles to their deployment in real-world applications [15, 35].

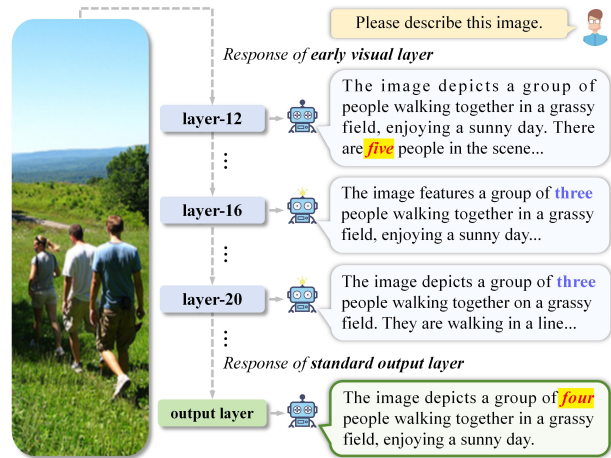


Figure 1. An example demonstrates where the LVLM provides a hallucinated response based on the features from standard visual output layer, yet correctly identifies the number of people in the image when relying on features from other visual hidden layers. The correct answer and hallucination are highlighted in blue and red, respectively.

Researchers have recently proposed various methods to address the hallucination issue in LVLMs. Most of these approaches aim to mitigate hallucinations by applying additional post-training steps [13, 21, 27, 28]. Some methods use post-hoc correction during the inference phase, often relying on an extra revision model [38, 47] or manual-crafted correction pipeline [44, 49]. However, these techniques typically encounter challenges, such as high computational costs, complex implementation, and limited scalability. Recently, a novel paradigm focuses on modifying the decoding strategy during the inference phase [8, 20, 41, 42, 46], which substantially reduces implementation costs. These methods typically assume that the language model is the primary source of hallucinations, suggesting that generated hallucinated content is mainly influenced by language priors or statistical biases [11, 20, 31, 41, 45, 50], leading to

discrepancies between the generated outputs and the visual content. However, tracing back to the origin of hallucinations, it is crucial to recognize that accurate and comprehensive visual input is a necessary condition for ensuring correct model reasoning. Building on this insight, we propose a bold conjecture: *Could hallucinations in LVLMs stem from underlying issues within the visual encoding process?*

Taking the counting task as an example, the extent of hallucination in LVLMs is closely tied to their ability to perceive visual information. As shown in Figure 1, LVLM produces incorrect answers when relying on features from the standard visual output layer. In contrast, they make correct inferences when using features from earlier visual hidden layers. This observation suggests the vision encoder successfully extracts key features from the image, particularly in earlier layers. However, as this information propagates toward the output layer, it may become distorted or subject to interference, resulting in errors in the final response.

Inspired by this finding, we propose a novel hallucination mitigation method: Visual-Layer Fusion Contrastive Decoding (VaLiD). This approach utilizes uncertainty as a guide for selecting visual hidden layers, and employs contrastive decoding to compare the reference distribution derived from visual hidden layers with the original distribution from the standard visual output layer. This contrastive process enables the model to self-correct distortions in the visual encoding process, ultimately increasing the probability of correct decoding and enhancing the reliability and accuracy of the generated text.

Our contribution are summarized as follows: (1) We highlight the significance of the vision encoder in LVLM inference stage and investigate LVLMs’ hallucinations from the perspective of visual encoding. (2) We demonstrate the existence of visual information distortion during encoding process across multiple LVLMs, showing its significant contribution to hallucinations in model responses. (3) We propose a training-free method, VaLiD, that leverages uncertainty to guide the construction of reference distributions, which are then compared with the original distribution to correct hallucinated responses. (4) Extensive experimental evaluations demonstrate that VaLiD effectively reduces hallucinations and enhances the reliability of generated text, achieving state-of-the-art performance compared to baseline methods.

## 2. Related Works

**Hallucination Mitigation in LVLMs.** In Large Vision-Language Models (LVLMs), content generated that is inconsistent with visual information is referred to as model hallucination. Various methods have been proposed to address this issue. Some approaches involve additional training steps to enhance the language model’s ability to interpret visual tokens, utilizing techniques such as auxiliary su-

pervision [5, 27] and reinforcement learning [37]. However, these methods inevitably rely on a large amount of annotated data and high training costs.

Meanwhile, some studies aim to mitigate hallucinations during the inference stage. Certain approaches [43, 44] apply post-hoc corrections to address hallucinated content; however, their effectiveness is often constrained by reliance on auxiliary models or manual-crafted correction pipeline. Other methods [5, 8, 10, 16, 20, 41, 42] intervene in the decoding strategy during token generation in the inference phase, avoiding additional training or auxiliary modules, thereby reducing the computational costs. Nonetheless, these approaches generally attribute hallucinations to statistical biases or prior knowledge within the language model, with limited attention to the impact of the visual encoding process on hallucinations. Our method addresses this gap by focusing on the visual encoding process, tracing hallucinations to their origins in the vision encoder and mitigating them through corrections in the visual output layer.

**Contrastive Decoding:** Contrastive decoding was initially developed to optimize the output probability distribution of language models [22, 32, 48] and has recently applied in LVLMs, where it improves model outputs by contrasting the conditional probabilities of responses to original versus reference inputs. Several methods have been employed to construct effective reference distributions, such as introducing uncertainty in inputs (e.g., VCD [20], ICD [41], etc.), contrastive models (e.g., IBD [50], M3ID [10], etc.), and data augmentation (e.g., RITUAL [42], VACoDe [19], etc.). Additionally, work represented by DoLa [6] explores leveraging knowledge across different hidden layers of language models, effectively enhancing the model’s reasoning capabilities on factual knowledge by contrasting information across layers. Our method, while also utilizing hidden layer information, specifically focuses on dealing with the potential distortions of visual information when it is transmitted across layers within the vision encoder. By applying contrastive techniques, our approach mitigates the negative effects of these distortions on visual information, thereby effectively reducing hallucinations in LVLMs.

## 3. Methodology

### 3.1. Visual Encoding Distortion Induces Hallucinations

In general, features derived from the standard visual output layer are effective for reasoning across multimodal tasks. However, as shown in Figure 1, they may not be the most accurate when addressing problems prone to hallucination, such as those involving attributes, relations, or existential semantics. This observation motivates further investigation into how the visual encoding process influences the model’s behavior with respect to hallucinations.

Model	bucket1	bucket2	bucket3	bucket4	bucket5	bucket6
LLaVA-v1.5 [30]	0.0	0.88	8.85	18.58	<b>33.63</b>	30.09
InstructBLIP [7]	16.13	16.13	33.87	61.29	<b>69.35</b>	54.84
Qwen-VL [2]	0.0	7.46	<b>14.93</b>	4.38	8.96	1.49

Table 1. We report the encoding distortion rate across the visual layers of three representative LVLMs by dividing all visual hidden layers into distinct buckets. A bucket is deemed correctly answered if the visual features within it enable accurate decoding by the LVLMs. Taking the counting task as an example [39], the question is framed as ‘‘How many [obj] are there in this image?’’

**Finding 1: Encoding Distortion in Visual Layers Causes Most Prediction Reversals.** To quantify the potential distortion in visual encoding process, we first analyze the decoding results of LVLMs regarding the early visual layers. Specifically, we introduce the Encoding Distortion Rate (EDR) to evaluate the statistics, which is defined as follows:  $\frac{S_i^+ \cap S_{so}^-}{S_{so}^-}$ , where  $S_i^+$  denotes the number of features in the  $i$ -th set of visual layers that can be decoded correctly, and  $S_{so}^-$  represents the number of incorrectly decoded features from the standard visual output layer. As shown in Table 1, there is a significant proportion of samples can be decoded correctly at the early visual hidden layers but unexpectedly decode wrongly at the standard output layer. Especially in bucket 5 of the InstructBLIP model (with layers ranging from 31 to 34), the EDR score reaches an astonishing 69.35%. This suggests that key visual information has become distorted during the forward process, negatively impacting the feature representation of the standard visual output layer and ultimately causing the model’s prediction to shift from correct to incorrect.

**Finding 2: Uncertainty as Indicator of Encoding Distortion.** Based on the above finding, it’s critical to identify which visual encoding layer is distorted. Inspired by [4, 33], we employ uncertainty to demonstrate the changes of visual information during its transmission through the hidden layers of the visual encoder. The uncertainty of the visual layer features, as defined in Eq. 1, is measured as the entropy of the next token’s probability when the LVLMs make predictions based on the current visual layer features.

$$H_{i,t} = - \sum_{y_t \in \mathcal{V}} P_\theta(y_t | v_i, x, y_{<t}) \log P_\theta(y_t | v_i, x, y_{<t}) \quad (1)$$

Here,  $\mathcal{V}$  is the vocabulary space,  $v_i$  denotes the visual features of the  $i$ -th layer,  $x$  denotes a query associated with image  $v$  and  $y_{<t}$  represents the generated tokens. We statistically analyze the relationship between the uncertainty of visual features across different layers and the decoding accuracy of the LVLm, as illustrated in Figure 2. Our findings reveal that hidden layers with wrong decoding results tend to have higher uncertainty, whereas layers with correct de-

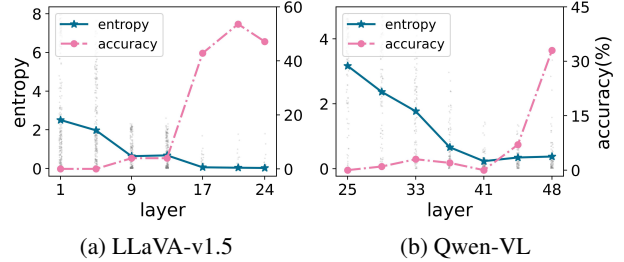


Figure 2. The trend of uncertainty and decoding accuracy as the number of layers increases. The nodes on the entropy curve represent the average entropy value across all questions within the current layer. It should be noted that LLaVA-v1.5 utilizes the feature from the penultimate layer of CLIP-ViT as the standard visual output.

coding exhibit relatively low uncertainty. This suggests that certain hidden layers with significant uncertainty impact the visual encoding process. These effects propagate from the previous layer to the subsequent layer, growing increasingly conspicuous during decoding, and eventually accumulating in the standard output layer, thus leading LVLMs to make erroneous inferences according to the distorted features.

### 3.2. Visual-Layer Fusion Contrastive Decoding

Building on previous findings, we observe that feature representations are affected by distortions originating from early visual layers with high uncertainty, ultimately leading to hallucinations during the LVLMs’ decoding process. To address this issue, we introduce Visual-Layer Fusion Contrastive Decoding (VaLiD). As shown in Figure 3, VaLiD effectively mitigates distortion effects in the visual encoding process by contrasting the probability distribution of features from the standard output layer with those from high-uncertainty layers. Our approach is training-free, providing correction solely during model inference stage.

**Uncertainty-guided Visual-Layer Fusion.** Given that uncertainty can indicate information distortion within the visual encoding process, we propose leveraging early visual layers with high uncertainty to improve output correction through contrastive decoding. However, directly relying on hidden layers with the highest uncertainty could lead the model to excessively depend on potentially unstable information from a single layer [6, 33]. To address this, we introduce a layer fusion approach to enhance the robustness of contrastive decoding. Specifically, at each time step, we dynamically select the top-k layers with the highest uncertainty to construct a candidate set of layers. To ensure computational efficiency, we partition the visual encoder’s layers into several buckets, allowing fusion within specific layer ranges, with the optimal bucket determined by the validation set (see Sec. 4.1 for implementation details). This dynamic layer selection strategy adaptively identifies

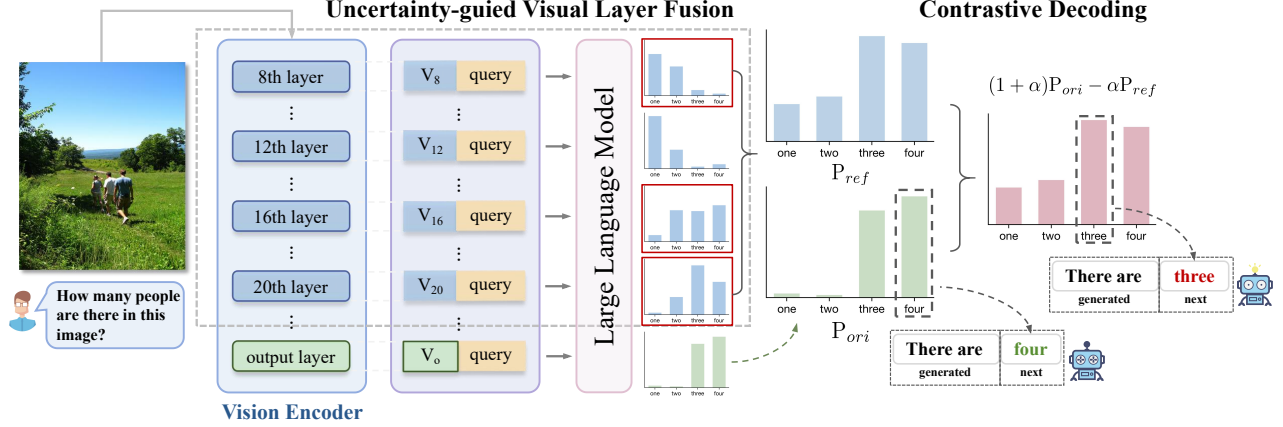


Figure 3. Overview of the VaLiD decoding process. At each time step, the LVLm auto-regressively samples the token  $y_t$  based on visual input, text query, and previously generated tokens. The probability distributions represented in **Green** and **Blue** correspond to decoding results from the standard visual output layer and early visual layers, respectively. The red boxes indicate that the probability distributions of the selected visual layers, which reflect the top-k uncertainty, will be used to calculate the reference distribution. The final corrected probability distribution, shown in **Red**, is obtained through contrastive decoding. For example, when asked about the number of people in the image, LVLm generates the correct decoding result, "three", instead of the incorrect "four" from the original distribution.

the most suitable set of early visual layers based on the next token, enhancing the effective use of visual information across layers. Through this bucketing and selection approach, we balance computational efficiency and decoding performance. Finally, we represent the reference probability distribution of the next token as a weighted average of the distributions derived from features of earlier layers, with each layer's uncertainty value serving as the weighting factor, as shown in Eq. 2.

$$P_{ref} = \sum_{i \in \mathcal{C}} \omega_i \cdot P_{\theta}(y_t | v_i, x, y_{<t})$$

$$\omega_i = \frac{\exp^{H_{i,t}}}{\sum_k^{|C|} \exp^{H_{k,t}}}$$
(2)

**Contrastive Decoding.** After obtaining (1) the next token distribution conditioned on the standard output layer features, denoted as  $P_{ori}$  and (2) the reference distribution, denoted as  $P_{ref}$ , we compute a new probability distribution by contrasting the differences between these two distributions [22, 26]. The contrastive result is presented in Eq. 3.

$$P_{valid} = (1 + \alpha)P_{ori} - \alpha \sum_{i \in \mathcal{C}} \omega_i \cdot P_{\theta}(y_t | v_i, x, y_{<t})$$
(3)

where  $\alpha$  is a positive coefficient to control the contrast intensity. A larger  $\alpha$  values indicate a stronger amplification of differences between the two distributions ( $\alpha = 0$  reduces to regular decoding). However, the newly generated distribution  $P_{valid}$  may mistakenly penalize valid outputs in  $P_{ori}$ , leading to decoding results that do not adhere to basic language standards and commonsense reasoning. To address

this issue, we adopt an adaptive reliability constraint following the approach of [18], as shown in Eq. 4.

$$\mathcal{V}_{head}(y_{<t}) = \{y_t \in \mathcal{V} | P_{\theta}(y_t | v, x, y_{<t}) \geq \beta \max_w p_{\theta}(w | v, x, y_{<t})\},$$

$$P_{valid}(y_t | v, x, y_{<t}) = 0, \text{ if } y_t \notin \mathcal{V}_{head}(y_{<t}),$$
(4)

If  $y_t$  is not in  $\mathcal{V}_{head}(y_{<t})$ , it indicates that the token has a very low probability under the original distribution, suggesting it is likely an unreasonable prediction. Therefore, we set the probability of the same position  $y_t$  in the corrected distribution to zero, preventing the score of these  $y_t$  tokens from being abnormally amplified after contrastive adjustment.

## 4. Experiment

### 4.1. Evaluation Setup

**LVLms:** We integrate our proposed method VaLiD with three representative LVLms: InstructBLIP-7B [7], LLaVA-1.5-7B [30], and Qwen-VL-7B [2]. Each model utilizes Vision Transformer (ViT) as the backbone of its visual encoder, but employs different pre-training strategies, such as Eva-ViT (39 layers) [9], CLIP (25 layers) [34], and ViT-bigG (49 layers), where the numbers indicate the layer count of the visual encoder. To ensure the efficiency of our method, instead of merging the distributions from all visual layers, we focus on a specific range of visual layer features as candidate layers for contrastive decoding. Following the approach inspired by DoLa, we partition the ViT layers into buckets and iden-

Dataset	Setup	Method	LLaVA-v1.5			InstructBLIP			Qwen-VL		
			Acc.↑	F1↑	Yes	Acc.↑	F1↑	Yes	Acc.↑	F1↑	Yes
MSCOCO [25]	Random	Vanilla	82.33	80.57	40.93	82.20	81.86	48.13	85.17	83.10	37.77
		VCD	87.23	86.19	42.43	84.37	83.80	46.50	87.17	85.65	39.43
		M3ID	86.53	85.18	40.87	79.77	78.66	44.83	85.97	83.99	37.63
		Ritual	85.80	83.81	37.73	85.33	83.76	40.33	85.40	83.06	36.20
		VaLiD	<b>88.60</b>	<b>87.67</b>	42.47	<b>85.93</b>	<b>84.51</b>	40.80	<b>88.10</b>	<b>86.86</b>	40.57
	Popular	Vanilla	81.10	79.48	42.10	79.10	79.30	50.97	84.73	82.70	38.27
		VCD	85.80	84.96	44.40	81.23	80.93	48.43	86.07	84.59	40.40
		M3ID	84.63	83.39	42.50	76.80	76.37	48.20	84.87	82.88	38.40
		Ritual	84.93	83.18	39.60	82.87	81.53	42.80	84.84	82.55	36.90
		VaLiD	<b>85.89</b>	<b>85.89</b>	44.00	<b>83.40</b>	<b>82.14</b>	43.93	<b>87.13</b>	<b>86.00</b>	41.93
	Adversarial	Vanilla	78.63	77.76	46.10	76.87	77.58	53.20	83.33	81.63	40.73
		VCD	81.40	80.84	47.07	78.53	78.69	50.73	84.27	83.00	42.53
		M3ID	81.70	80.80	45.30	74.93	75.52	52.40	83.23	81.45	40.37
		Ritual	82.60	81.05	41.80	80.77	79.73	44.90	82.80	80.45	38.00
		VaLiD	<b>83.67</b>	<b>83.43</b>	48.60	<b>81.43</b>	<b>80.53</b>	45.36	<b>84.43</b>	<b>83.55</b>	44.63
A-OKVQA [36]	Random	Vanilla	85.53	85.11	47.13	80.50	81.49	55.37	86.80	85.58	41.53
		VCD	87.90	87.72	49.40	83.13	83.75	53.80	87.80	86.84	42.73
		M3ID	87.27	86.86	46.93	78.53	78.36	49.20	87.43	86.21	41.10
		Ritual	89.27	88.69	44.93	84.53	83.73	45.07	86.10	84.41	39.16
		VaLiD	<b>89.93</b>	<b>89.85</b>	49.20	<b>87.00</b>	<b>86.81</b>	48.53	<b>88.70</b>	<b>88.03</b>	44.43
	Popular	Vanilla	81.43	81.29	49.23	76.57	78.48	58.90	86.73	85.37	40.67
		VCD	82.47	83.03	53.33	78.76	80.36	58.10	87.53	86.66	43.47
		M3ID	83.53	83.48	49.67	76.67	77.08	51.80	87.27	86.09	41.53
		Ritual	<b>86.60</b>	86.38	48.40	81.83	81.47	48.03	85.77	83.99	38.90
		VaLiD	86.03	<b>86.47</b>	53.23	<b>82.90</b>	<b>82.48</b>	53.30	<b>88.90</b>	<b>88.32</b>	45.03
	Adversarial	Vanilla	75.47	76.81	55.80	70.43	74.34	65.23	80.87	80.17	46.47
		VCD	76.60	78.60	59.33	72.83	76.08	63.57	81.80	81.59	48.87
		M3ID	76.97	78.55	57.37	68.23	71.16	60.17	81.40	80.80	46.87
		Ritual	79.07	79.81	53.67	74.63	75.79	54.77	80.83	79.66	44.23
		VaLiD	<b>79.13</b>	<b>81.13</b>	60.60	<b>75.60</b>	<b>77.78</b>	59.80	<b>82.26</b>	<b>82.45</b>	51.07
GQA [17]	Random	Vanilla	84.70	83.97	45.43	79.17	80.47	56.70	84.40	83.27	43.27
		VCD	87.90	87.67	48.10	82.10	82.75	53.77	86.73	85.94	44.33
		M3ID	86.20	85.70	46.53	78.37	78.10	48.77	85.93	84.94	43.40
		Ritual	87.93	87.14	43.87	83.26	82.23	44.13	85.80	84.42	41.13
		VaLiD	<b>88.70</b>	<b>88.63</b>	49.37	<b>85.20</b>	<b>84.91</b>	48.07	<b>89.97</b>	<b>89.45</b>	45.10
	Popular	Vanilla	77.83	78.23	51.83	74.23	76.71	60.63	80.50	80.03	47.63
		VCD	80.07	81.10	55.47	76.63	78.60	59.17	82.33	82.09	48.67
		M3ID	78.60	78.84	51.13	74.07	74.92	53.40	81.07	80.29	46.07
		Ritual	82.08	82.58	48.73	<b>79.33</b>	79.29	49.80	82.56	81.26	43.03
		VaLiD	<b>82.20</b>	<b>83.05</b>	55.00	78.37	<b>79.40</b>	55.03	<b>84.40</b>	<b>84.46</b>	50.40
	Adversarial	Vanilla	75.70	76.57	53.70	71.13	74.69	64.07	79.33	79.17	49.20
		VCD	76.30	78.08	58.10	73.27	76.60	64.27	81.10	81.11	50.03
		M3ID	77.20	78.08	54.00	68.80	71.06	57.80	79.83	79.61	48.90
		Ritual	<b>80.10</b>	80.47	51.90	74.67	75.75	54.47	80.33	79.31	45.06
		VaLiD	78.83	<b>80.52</b>	58.63	<b>75.23</b>	<b>76.99</b>	57.63	<b>82.33</b>	<b>82.74</b>	52.33

Table 2. **Results on POPE benchmark.** VaLiD consistently outperforms the contrastive decoding baseline: VCD [20], M3ID [10] and Ritual [42]. The best performances within each setting are **bolded**. VCD, M3ID and Ritual are reproduced within our evaluation setting.

tify one bucket as the candidate layer set using the validation set. For the 25-layer LLaVA-v1.5-7B, we select layers [13, 15, 17, 19, 21, 23, 25]. For the 39-layer InstructBLIP-7B, we choose layers [29, 31, 33, 35, 37, 39]. For the 48-

layer Qwen-VL-7B, we utilize layers [45, 46, 47, 48, 49].

**Datasets and Benchmarks:** We evaluate our approach using three benchmarks: (1) POPE [24], which proposes a method to evaluate object hallucination in LVLMS

Model	Method	State		Action		Number		Relation	
		Acc.↑	F1↑	Acc.↑	F1↑	Acc.↑	F1↑	Acc.↑	F1↑
LLaVA-v1.5	Vanilla	69.77	69.20	78.91	78.00	71.81	70.47	58.59	53.91
	VCD	71.87	71.31	81.57	81.61	72.54	72.50	60.40	56.56
	M3ID	70.45	69.65	83.96	83.61	74.23	73.06	58.05	53.34
	Ritual	<b>74.22</b>	73.28	85.35	84.74	<b>80.60</b>	79.06	54.99	39.35
	VaLiD	73.59	<b>73.50</b>	<b>85.35</b>	<b>85.57</b>	78.57	<b>79.50</b>	<b>65.87</b>	<b>63.68</b>
InstructBLIP	Vanilla	69.37	69.80	73.86	75.73	69.64	73.02	58.11	61.68
	VCD	<b>73.95</b>	<b>74.53</b>	77.53	79.30	73.89	77.49	60.40	65.04
	M3ID	64.82	62.51	77.15	75.90	65.97	68.98	58.29	62.81
	Ritual	69.50	64.71	80.18	78.24	74.23	76.84	<b>67.37</b>	<b>70.15</b>
	VaLiD	72.86	72.08	<b>81.06</b>	<b>82.06</b>	<b>79.78</b>	<b>81.40</b>	63.46	64.81
Qwen-VL	Vanilla	75.90	72.60	83.08	81.18	82.38	80.92	53.73	39.28
	VCD	77.50	74.75	85.1	83.88	83.59	82.79	56.85	45.44
	M3ID	76.41	73.36	86.61	85.36	83.69	82.59	53.79	39.69
	Ritual	76.55	73.22	83.71	81.49	85.96	84.76	49.46	25.11
	VaLiD	<b>79.30</b>	<b>78.41</b>	<b>87.75</b>	<b>87.48</b>	<b>86.05</b>	<b>86.68</b>	<b>62.92</b>	<b>58.56</b>

Table 3. **Results on AMBER benchmark.** The AMBER dataset includes attribute-level hallucinations, which contains state attributes (e.g., color, shape), action attributes (e.g., actions performed by humans or animals in the image), and numerical attributes (typically noted when an object appears multiple times in the image). Additionally, it includes relation-level hallucinations, which refers to whether there is direct contact between two objects in an image.

by answering yes/no questions about object existence. This benchmark includes evaluations across three datasets: MS-COCO [25], A-OKVQA [36], and GQA [17], each contains three subsets—random, popular, and adversarial—corresponding to the sampling strategies used to create negative samples. These subsets present increasing levels of difficulty, providing a progressive assessment of whether LVLMs tend to generate specific objects erroneously. (2) MME [12] is a comprehensive benchmark for evaluating LVLMs, encompassing 14 tasks across various dimensions. We follow the experimental settings in VCD, using the existence and count subsets for object-level hallucination evaluation, and the location and color subsets for attribute-level hallucination evaluation. Additionally, we report LVLMs’ performance across the remaining 10 tasks to examine whether the contrastive decoding method affects the model’s reasoning capability. (3) AMBER [39] provides fine-grained annotation information, specifically 1,004 images and corresponding 15,200 annotations, covering three types of model hallucinations, namely existence, attribute, and relation hallucinations.

**Metrics:** We follow the official implementations for the POPE, MME, and AMBER benchmarks. Specifically, hallucination evaluation on these benchmarks is generally defined as a binary classification task. We utilize multiple metrics, including Accuracy, Precision, Recall, and F1-score. Due to space constraints, Precision and Recall scores are provided in the supplementary material A. Additionally, we report the *Yes* ratio in POPE to further showcase LVLMs’ behavior, where *Yes* ratio denotes the proportion of answering ‘Yes’ to the given question.

**Baseline Settings:** Unlike post-hoc hallucination mitigation methods, our approach modifies the model’s decoding strategy. Therefore, we select VCD [20], M3ID [10] and Ritual [42] as baseline methods. Both VCD and M3ID adopt contrastive decoding strategy based on prior knowledge, where hallucinations typically originate from language models. While Ritual preserves consistent visual representations through a data augmentation strategy. We also report the evaluation results of the vanilla model, which does not employ any specific decoding strategy. All baseline methods are compared under our evaluation setting to ensure the fairness and consistency of the experiments.

## 4.2. Experimental Results

**Results on POPE:** Table 2 presents the overall performance of VaLiD in comparison with other baseline methods on the POPE benchmark. The experimental results indicate that our method significantly enhances performance across three LVLMs compared to the vanilla model. This improvement suggests that by eliminating high-uncertainty layer probability distributions from the standard visual output, we can effectively mitigate adverse effects caused by encoding distortion. Additionally, VaLiD outperforms other methods in reducing hallucinations across various models and datasets, suggesting that, beyond addressing hallucinations from the language model side, the correctness of visual encoding also plays a crucial role in mitigating hallucinations.

Moreover, all LVLMs exhibit performance degradation as we move from the random setting to the popular setting, with a further decline under the adversarial setting. Compared to other methods, VaLiD maintains a relatively sig-

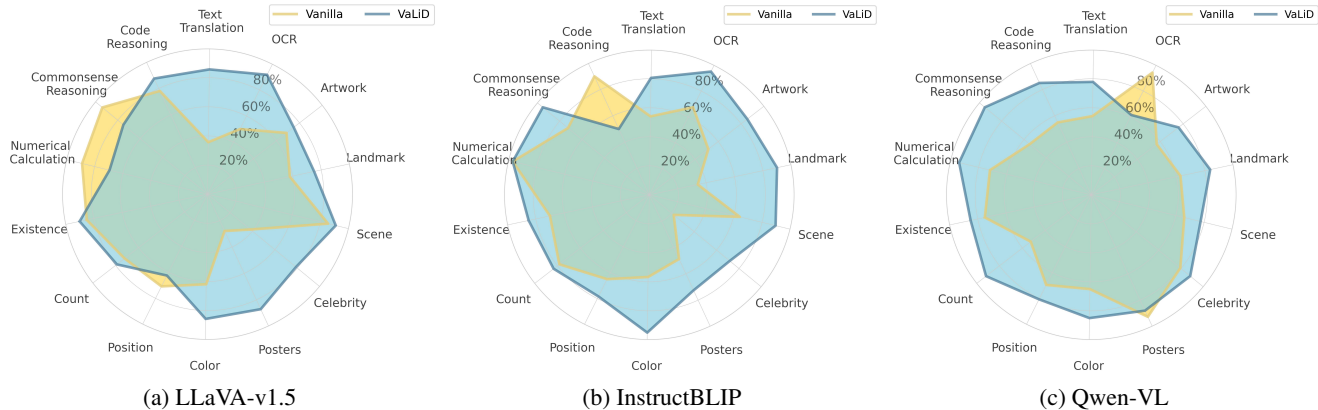


Figure 4. **Results of MME benchmark.** LVLMs with VaLiD achieve the best performance in **11** out of 14 categories for LLaVA-v1.5, **13** out of 14 categories for InstructBLIP, and **12** out of 14 categories for Qwen-VL. VaLiD not only mitigates hallucinations but also enhances the overall capabilities of LVLMs. Detailed results are provided in the supplementary material B.

Type	Method	MSCOCO			A-OKVQA			GQA		
		Acc.↑	F1↑	Yes	Acc.↑	F1↑	Yes	Acc.↑	F1↑	Yes
Random	$\mathbb{P}_{\text{vcd}} \circ \mathbb{P}_{\text{valid}}$	89.00 <sub>(1.09)</sub>	88.36 <sub>(1.43)</sub>	44.47	<b>90.43</b> <sub>(1.52)</sub>	<b>90.61</b> <sub>(1.83)</sub>	51.90	<b>89.00</b> <sub>(0.70)</sub>	<b>89.10</b> <sub>(0.95)</sub>	50.93
	$\mathbb{P}_{\text{valid}} \circ \mathbb{P}_{\text{vcd}}$	<b>89.40</b> <sub>(1.49)</sub>	<b>88.59</b> <sub>(1.66)</sub>	42.93	88.93 <sub>(0.02)</sub>	88.06 <sub>(-0.73)</sub>	42.67	88.70 <sub>(0.40)</sub>	87.83 <sub>(-0.32)</sub>	42.83
Popular	$\mathbb{P}_{\text{vcd}} \circ \mathbb{P}_{\text{valid}}$	86.50 <sub>(0.66)</sub>	86.01 <sub>(0.59)</sub>	46.50	85.87 <sub>(1.62)</sub>	<b>86.73</b> <sub>(1.98)</sub>	56.47	82.33 <sub>(1.20)</sub>	83.60 <sub>(1.53)</sub>	57.73
	$\mathbb{P}_{\text{valid}} \circ \mathbb{P}_{\text{vcd}}$	<b>87.23</b> <sub>(1.39)</sub>	<b>86.50</b> <sub>(1.08)</sub>	44.57	<b>86.90</b> <sub>(2.65)</sub>	86.17 <sub>(1.42)</sub>	44.70	<b>87.67</b> <sub>(6.54)</sub>	<b>86.98</b> <sub>(4.91)</sub>	44.73
Adversarial	$\mathbb{P}_{\text{vcd}} \circ \mathbb{P}_{\text{valid}}$	83.07 <sub>(0.54)</sub>	83.02 <sub>(0.89)</sub>	49.73	77.90 <sub>(0.04)</sub>	80.61 <sub>(0.75)</sub>	63.97	77.17 <sub>(-0.40)</sub>	79.52 <sub>(0.22)</sub>	61.50
	$\mathbb{P}_{\text{valid}} \circ \mathbb{P}_{\text{vcd}}$	<b>83.93</b> <sub>(1.40)</sub>	<b>83.49</b> <sub>(1.36)</sub>	47.33	<b>83.80</b> <sub>(5.94)</sub>	<b>83.45</b> <sub>(3.59)</sub>	47.87	<b>83.93</b> <sub>(6.37)</sub>	<b>83.56</b> <sub>(4.26)</sub>	47.73

Table 4. Results of the POPE benchmark on LLaVA-v1.5. The values in brackets indicate the average improvement achieved by the method ensemble in the specified order, relative to VCD and VaLiD individually.

nificant improvement in both the popular and adversarial sampling conditions, where other baseline methods exhibit varying levels of decline under highly correlated sampling conditions. For example, on the GQA dataset, VCD’s improvements over the vanilla model across the three sampling strategies are 3.2, 2.24, and 0.6, respectively, while VaLiD’s improvements are 4, 4.37, and 3.13, demonstrating greater stability across the sampling methods. This suggests that our method enables LVLMs to better counteract interference from related data (e.g., frequently co-occurring objects) by correcting the adverse effects of inaccurate visual information, allowing LVLMs to more accurately understand object relationships.

**Results on AMBER:** Our evaluation on AMBER dataset demonstrates the performance of each decoding strategy in mitigating various types of hallucinations beyond object existence. As shown in Table 3, VaLiD exhibits strong competitiveness across various tasks. Notably, for questions involving object actions and number attributes, VaLiD outperforms a series of contrastive decoding methods that rely on data augmentation, such as VCD and Ritual. This advantage arises from VaLiD’s ability to avoid additional biases

introduced by data augmentation, which can alter the attribute semantics of images. For example, in VCD, adding Gaussian noise can obscure small target objects, while in Ritual, random cropping may inadvertently remove target objects. However, we observe that VaLiD performs less effectively on InstructBLIP for state and relation-level hallucinations, highlighting that state and relational reasoning remains a challenging task for InstructBLIP, with limited improvement achieved through VaLiD. Despite this, VaLiD still surpasses most baseline methods.

**Results on MME:** As shown in Figure 4, VaLiD significantly enhances performance in most perceptual and cognitive tasks across all three LVLMs, indicating its effectiveness in mitigating hallucinations without compromising the model’s inherent capabilities. Notably, VaLiD even appears to boost perceptual and cognitive performance in specific tasks; for example, in the posters task, VaLiD outperforms the vanilla model by 29.59 in LLaVA-v1.5, and in the text translation task, VaLiD surpasses the vanilla model by 40 in Qwen-VL. However, certain cognitive tasks, such as code reasoning and numerical calculation, show better performance with the vanilla model. We hypothesize that this may

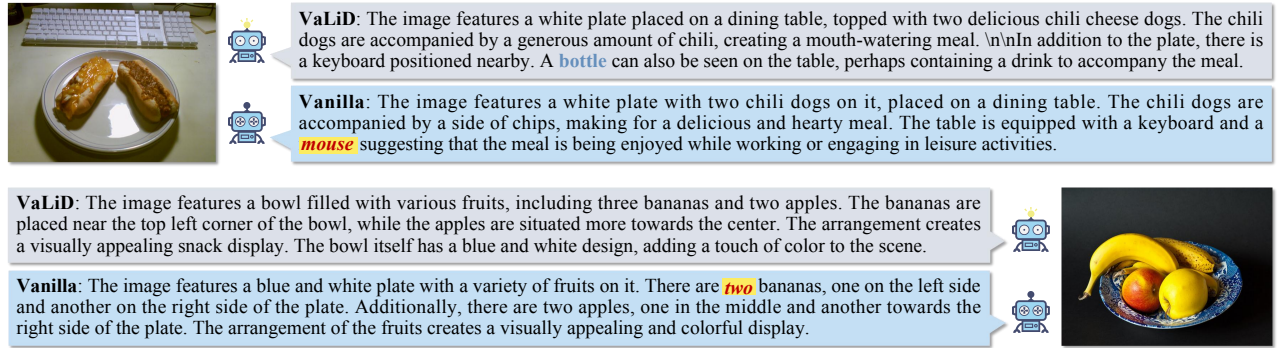


Figure 5. Illustration of hallucination correction by our proposed VaLiD with two examples from AMBER dataset [39]. Hallucinated objects from vanilla decoding are highlighted in **red**.

be due to the inherent challenges posed by statistical biases and language priors affecting LVLMs, which might not be fully addressed from vision encoder perspective.

### 4.3. Further Analysis

**VaLiD is more compatible than VCD.** Since VaLiD constructs the reference distribution from a visual encoding perspective, it is inherently compatible with other methods that derive the reference distribution from language models. Here, we investigate the integration of VCD with VaLiD to evaluate its impact on mitigating hallucinations. VCD attributes hallucinations to the language model itself, amplifying language priors and statistical biases by introducing visual uncertainty and subsequently applying a contrastive approach to mitigate hallucinations. However, the sequence in which VCD and VaLiD are applied presents a challenge, as different orders produce distinct decoding strategies. As stated in Claim 1, the variation in probability distributions resulting from different application orders is proportional to the difference in reference distributions constructed by the two methods. The proof can be found in the supplementary material C.

**Claim 1** Let  $\mathbb{P}_{valid} \circ \mathbb{P}_{vcd}$  and  $\mathbb{P}_{vcd} \circ \mathbb{P}_{valid}$  represent the application of VCD and VaLiD in different sequences. Assuming truncation effects are negligible, then we have

$$\|\mathbb{P}_{valid} \circ \mathbb{P}_{vcd} - \mathbb{P}_{vcd} \circ \mathbb{P}_{valid}\| = \mathcal{K}|P_{noi} - P_{ent}|$$

where  $\mathbb{P}$  indicate an operator formed as  $(1 + \alpha)P_{ori} - \alpha P_{ref}$ ,  $\circ$  represents the composition operator,  $P_{noi}$  and  $P_{ent}$  denote the reference distribution construct by VCD and VaLiD, respectively,  $\mathcal{K}$  denotes a constant value.

We evaluate the impact of order choices on alleviating model hallucinations using the POPE benchmark with LLaVA-v1.5. As shown in Table 4, in most cases, applying VaLiD after VCD results in higher accuracy compared to the vanilla model, VCD alone, or VaLiD alone. In

contrast, applying VCD after VaLiD yields accuracy nearly equivalent to VCD alone, falling short of the performance achieved by VaLiD alone. This outcome demonstrates the excellent compatibility of our approach, with improved performance achieved when VaLiD is integrated with VCD.

**Case studies on AMBER.** Figure 5 presents two case studies that illustrate how vanilla decoding results in object hallucinations, while VaLiD generates responses more closely aligned with the visual content. In these examples, a mouse often co-occurring with a keyboard and stacked bananas lead the model to produce hallucinated objects. In contrast, VaLiD effectively mitigates these issues. Additionally, VaLiD successfully identifies a bottle in the upper left corner in the first case—a commonly overlooked object by most LVLMs. More cases can be found in the supplementary material D.

## 5. Conclusion

In this paper, we introduce Visual Layer Fusion Contrastive Decoding (VaLiD), a novel, training-free method for mitigating hallucinations in LVLMs. Our approach highlights the critical role of the visual encoding process, showing that distorted visual information may induce hallucinations. We leverage probability distributions from hidden layers to correct distortions in the standard output layer of the visual encoder, thereby enhancing the reliability of the generated text. Extensive experimental results validate the effectiveness of VaLiD across multiple datasets and LVLMs.

In our exploration of the visual encoder’s hidden layers, we observed distortions in visual information and their correlation with uncertainty. In future work, we plan to investigate the underlying causes of these distortions. These findings also motivate us to further explore the inner workings of the visual encoder and the impact of visual information on the multimodal task reasoning, beyond hallucinations.



## References

- [1] Stanislaw Antol, Aishwarya Agrawal, Jiasen Lu, Margaret Mitchell, Dhruv Batra, C Lawrence Zitnick, and Devi Parikh. Vqa: Visual question answering. In *Proceedings of the IEEE international conference on computer vision*, pages 2425–2433, 2015. 1
- [2] Jinze Bai, Shuai Bai, Shusheng Yang, Shijie Wang, Sinan Tan, Peng Wang, Junyang Lin, Chang Zhou, and Jingren Zhou. Qwen-vl: A versatile vision-language model for understanding, localization, text reading, and beyond, 2023. 1, 3, 4
- [3] Sébastien Bubeck, Varun Chandrasekaran, Ronen Eldan, Johannes Gehrke, Eric Horvitz, Ece Kamar, Peter Lee, Yin Tat Lee, Yuanzhi Li, Scott Lundberg, et al. Sparks of artificial general intelligence: Early experiments with gpt-4. *arXiv preprint arXiv:2303.12712*, 2023. 1
- [4] Shiqi Chen, Miao Xiong, Junteng Liu, Zhengxuan Wu, Teng Xiao, Siyang Gao, and Junxian He. In-context sharpness as alerts: An inner representation perspective for hallucination mitigation. *arXiv preprint arXiv:2403.01548*, 2024. 3
- [5] Zhaorun Chen, Zhuokai Zhao, Hongyin Luo, Huaxiu Yao, Bo Li, and Jiawei Zhou. Halc: Object hallucination reduction via adaptive focal-contrast decoding. *arXiv preprint arXiv:2403.00425*, 2024. 2
- [6] Yung-Sung Chuang, Yujia Xie, Hongyin Luo, Yoon Kim, James Glass, and Pengcheng He. Dola: Decoding by contrasting layers improves factuality in large language models, 2024. 2, 3
- [7] Wenliang Dai, Junnan Li, Dongxu Li, Anthony Meng Huat Tiong, Junqi Zhao, Weisheng Wang, Boyang Li, Pascale Fung, and Steven Hoi. Instructblip: Towards general-purpose vision-language models with instruction tuning, 2023. 1, 3, 4
- [8] Ailin Deng, Zhirui Chen, and Bryan Hooi. Seeing is believing: Mitigating hallucination in large vision-language models via clip-guided decoding, 2024. 1, 2
- [9] Yuxin Fang, Wen Wang, Binhui Xie, Quan Sun, Ledell Wu, Xinggang Wang, Tiejun Huang, Xinlong Wang, and Yue Cao. Eva: Exploring the limits of masked visual representation learning at scale, 2022. 4
- [10] Alessandro Favero, Luca Zancato, Matthew Trager, Sidharth Choudhary, Pramuditha Perera, Alessandro Achille, Ashwin Swaminathan, and Stefano Soatto. Multi-modal hallucination control by visual information grounding. In *Proceedings of the IEEE/CVF Conference on Computer Vision and Pattern Recognition*, pages 14303–14312, 2024. 2, 5, 6, 1, 3, 4
- [11] Alessandro Favero, Luca Zancato, Matthew Trager, Sidharth Choudhary, Pramuditha Perera, Alessandro Achille, Ashwin Swaminathan, and Stefano Soatto. Multi-modal hallucination control by visual information grounding. In *Proceedings of the IEEE/CVF Conference on Computer Vision and Pattern Recognition*, pages 14303–14312, 2024. 1
- [12] Chaoyou Fu, Peixian Chen, Yunhang Shen, Yulei Qin, Mengdan Zhang, Xu Lin, Jinrui Yang, Xiawu Zheng, Ke Li, Xing Sun, Yunsheng Wu, and Rongrong Ji. Mme: A comprehensive evaluation benchmark for multimodal large language models, 2024. 6
- [13] Anisha Gunjal, Jihan Yin, and Erhan Bas. Detecting and preventing hallucinations in large vision language models. In *Proceedings of the AAAI Conference on Artificial Intelligence*, pages 18135–18143, 2024. 1
- [14] Anisha Gunjal, Jihan Yin, and Erhan Bas. Detecting and preventing hallucinations in large vision language models. In *Proceedings of the AAAI Conference on Artificial Intelligence*, pages 18135–18143, 2024. 1
- [15] Lei Huang, Weijiang Yu, Weitao Ma, Weihong Zhong, Zhangyin Feng, Haotian Wang, Qianglong Chen, Weihua Peng, Xiaocheng Feng, Bing Qin, and Ting Liu. A survey on hallucination in large language models: Principles, taxonomy, challenges, and open questions, 2023. 1
- [16] Qidong Huang, Xiaoyi Dong, Pan Zhang, Bin Wang, Conghui He, Jiaqi Wang, Dahua Lin, Weiming Zhang, and Nenghai Yu. Opera: Alleviating hallucination in multimodal large language models via over-trust penalty and retrospection-allocation. In *Proceedings of the IEEE/CVF Conference on Computer Vision and Pattern Recognition*, pages 13418–13427, 2024. 2
- [17] Drew A Hudson and Christopher D Manning. Gqa: A new dataset for real-world visual reasoning and compositional question answering. In *Proceedings of the IEEE/CVF conference on computer vision and pattern recognition*, pages 6700–6709, 2019. 1, 5, 6, 2, 3, 4
- [18] Chaoya Jiang, Haiyang Xu, Mengfan Dong, Jiaying Chen, Wei Ye, Ming Yan, Qinghao Ye, Ji Zhang, Fei Huang, and Shikun Zhang. Hallucination augmented contrastive learning for multimodal large language model. In *Proceedings of the IEEE/CVF Conference on Computer Vision and Pattern Recognition*, pages 27036–27046, 2024. 4
- [19] Sihyeon Kim, Boryeong Cho, Sangmin Bae, Sumyeong Ahn, and Se-Young Yun. Vacode: Visual augmented contrastive decoding. *arXiv preprint arXiv:2408.05337*, 2024. 2
- [20] Sicong Leng, Hang Zhang, Guanzheng Chen, Xin Li, Shijian Lu, Chunyan Miao, and Lidong Bing. Mitigating object hallucinations in large vision-language models through visual contrastive decoding. In *Proceedings of the IEEE/CVF Conference on Computer Vision and Pattern Recognition*, pages 13872–13882, 2024. 1, 2, 5, 6, 3, 4
- [21] Lei Li, Yuwei Yin, Shicheng Li, Liang Chen, Peiyi Wang, Shuhuai Ren, Mukai Li, Yazheng Yang, Jingjing Xu, Xu Sun, et al. A large-scale dataset towards multi-modal multilingual instruction tuning. *arXiv preprint arXiv:2306.04387*, 3, 2023. 1
- [22] Xiang Lisa Li, Ari Holtzman, Daniel Fried, Percy Liang, Jason Eisner, Tatsunori Hashimoto, Luke Zettlemoyer, and Mike Lewis. Contrastive decoding: Open-ended text generation as optimization. *arXiv preprint arXiv:2210.15097*, 2022. 2, 4
- [23] Yifan Li, Yifan Du, Kun Zhou, Jinpeng Wang, Wayne Xin Zhao, and Ji-Rong Wen. Evaluating object hallucination in large vision-language models. *arXiv preprint arXiv:2305.10355*, 2023. 1

- [24] Yifan Li, Yifan Du, Kun Zhou, Jinpeng Wang, Wayne Xin Zhao, and Ji-Rong Wen. Evaluating object hallucination in large vision-language models. *arXiv preprint arXiv:2305.10355*, 2023. 5, 1
- [25] Tsung-Yi Lin, Michael Maire, Serge Belongie, James Hays, Pietro Perona, Deva Ramanan, Piotr Dollár, and C Lawrence Zitnick. Microsoft coco: Common objects in context. In *Computer Vision—ECCV 2014: 13th European Conference, Zurich, Switzerland, September 6–12, 2014, Proceedings, Part V 13*, pages 740–755. Springer, 2014. 5, 6, 2, 3, 4
- [26] Alisa Liu, Maarten Sap, Ximing Lu, Swabha Swayamdipta, Chandra Bhagavatula, Noah A. Smith, and Yejin Choi. Dexperts: Decoding-time controlled text generation with experts and anti-experts, 2021. 4
- [27] Fuxiao Liu, Kevin Lin, Linjie Li, Jianfeng Wang, Yaser Yacoob, and Lijuan Wang. Mitigating hallucination in large multi-modal models via robust instruction tuning. In *The Twelfth International Conference on Learning Representations*, 2023. 1, 2
- [28] Fuxiao Liu, Kevin Lin, Linjie Li, Jianfeng Wang, Yaser Yacoob, and Lijuan Wang. Aligning large multi-modal model with robust instruction tuning. *arXiv preprint arXiv:2306.14565*, 2023. 1
- [29] Haotian Liu, Chunyuan Li, Qingyang Wu, and Yong Jae Lee. Visual instruction tuning, 2023. 1
- [30] Haotian Liu, Chunyuan Li, Yuheng Li, and Yong Jae Lee. Improved baselines with visual instruction tuning, 2024. 3, 4
- [31] Hanchao Liu, Wenyan Xue, Yifei Chen, Dapeng Chen, Xiutian Zhao, Ke Wang, Liping Hou, Rongjun Li, and Wei Peng. A survey on hallucination in large vision-language models. *arXiv preprint arXiv:2402.00253*, 2024. 1
- [32] Sean O’Brien and Mike Lewis. Contrastive decoding improves reasoning in large language models. *arXiv preprint arXiv:2309.09117*, 2023. 2
- [33] Zexuan Qiu, Zijing Ou, Bin Wu, Jingjing Li, Aiwei Liu, and Irwin King. Entropy-based decoding for retrieval-augmented large language models. *arXiv preprint arXiv:2406.17519*, 2024. 3
- [34] Alec Radford, Jong Wook Kim, Chris Hallacy, Aditya Ramesh, Gabriel Goh, Sandhini Agarwal, Girish Sastry, Amanda Askell, Pamela Mishkin, Jack Clark, Gretchen Krueger, and Ilya Sutskever. Learning transferable visual models from natural language supervision, 2021. 4
- [35] Vipula Rawte, Amit Sheth, and Amitava Das. A survey of hallucination in large foundation models. *arXiv preprint arXiv:2309.05922*, 2023. 1
- [36] Dustin Schwenk, Apoorv Khandelwal, Christopher Clark, Kenneth Marino, and Roozbeh Mottaghi. A-okvqa: A benchmark for visual question answering using world knowledge. In *European conference on computer vision*, pages 146–162. Springer, 2022. 1, 5, 6, 2, 3, 4
- [37] Zhiqing Sun, Sheng Shen, Shengcao Cao, Haotian Liu, Chunyuan Li, Yikang Shen, Chuang Gan, Liang-Yan Gui, Yu-Xiong Wang, Yiming Yang, et al. Aligning large multi-modal models with factually augmented rlhf. *arXiv preprint arXiv:2309.14525*, 2023. 2
- [38] David Wan, Jaemin Cho, Elias Stengel-Eskin, and Mohit Bansal. Contrastive region guidance: Improving grounding in vision-language models without training. *arXiv preprint arXiv:2403.02325*, 2024. 1
- [39] Junyang Wang, Yuhang Wang, Guohai Xu, Jing Zhang, Yukai Gu, Haitao Jia, Ming Yan, Ji Zhang, and Jitao Sang. An llm-free multi-dimensional benchmark for mllms hallucination evaluation. *arXiv preprint arXiv:2311.07397*, 2023. 3, 6, 8, 1, 5
- [40] Kaiye Wang, Qiyue Yin, Wei Wang, Shu Wu, and Liang Wang. A comprehensive survey on cross-modal retrieval. *arXiv preprint arXiv:1607.06215*, 2016. 1
- [41] Xintong Wang, Jingheng Pan, Liang Ding, and Chris Bie-mann. Mitigating hallucinations in large vision-language models with instruction contrastive decoding. *arXiv preprint arXiv:2403.18715*, 2024. 1, 2
- [42] Sangmin Woo, Jaehyuk Jang, Donguk Kim, Yubin Choi, and Changick Kim. Ritual: Random image transformations as a universal anti-hallucination lever in vlms. *arXiv preprint arXiv:2405.17821*, 2024. 1, 2, 5, 6, 3, 4
- [43] Junfei Wu, Qiang Liu, Ding Wang, Jinghao Zhang, Shu Wu, Liang Wang, and Tieniu Tan. Logical closed loop: Uncovering object hallucinations in large vision-language models. *arXiv preprint arXiv:2402.11622*, 2024. 2
- [44] Shukang Yin, Chaoyou Fu, Sirui Zhao, Tong Xu, Hao Wang, Dianbo Sui, Yunhang Shen, Ke Li, Xing Sun, and Enhong Chen. Woodpecker: Hallucination correction for multimodal large language models. *arXiv preprint arXiv:2310.16045*, 2023. 1, 2
- [45] Yi-Fan Zhang, Weichen Yu, Qingsong Wen, Xue Wang, Zhang Zhang, Liang Wang, Rong Jin, and Tieniu Tan. Debiasing large visual language models. *arXiv preprint arXiv:2403.05262*, 2024. 1
- [46] Linxi Zhao, Yihe Deng, Weitong Zhang, and Quanquan Gu. Mitigating object hallucination in large vision-language models via classifier-free guidance. *arXiv preprint arXiv:2402.08680*, 2024. 1
- [47] Linxi Zhao, Yihe Deng, Weitong Zhang, and Quanquan Gu. Mitigating object hallucination in large vision-language models via classifier-free guidance. *arXiv preprint arXiv:2402.08680*, 2024. 1
- [48] Zheng Zhao, Emilio Monti, Jens Lehmann, and Haytham Assem. Enhancing contextual understanding in large language models through contrastive decoding. In *NAACL 2024*, 2024. 2
- [49] Yiyang Zhou, Chenhang Cui, Jaehong Yoon, Linjun Zhang, Zhun Deng, Chelsea Finn, Mohit Bansal, and Huaxiu Yao. Analyzing and mitigating object hallucination in large vision-language models. *arXiv preprint arXiv:2310.00754*, 2023. 1
- [50] Lanyun Zhu, Deyi Ji, Tianrun Chen, Peng Xu, Jieping Ye, and Jun Liu. Ibd: Alleviating hallucinations in large vision-language models via image-biased decoding, 2024. 1, 2

# VaLiD: Mitigating the Hallucination of Large Vision Language Models by Visual Layer Fusion Contrastive Decoding

## Supplementary Material

### A. Additional Numerical Results on POPE

Table 5, Table 6 and Table 7 provide the detail numerical results of POPE, including accuracy, precision, recall, f1-score and yes ratio.

### B. Numerical Results of VaLiD on MME

In this section, we evaluate the impact of various decoding strategies on the model’s original performance while mitigating hallucinations, using the MME dataset. As shown in Table 8, VaLiD consistently outperforms the vanilla model across most tasks, particularly in reasoning tasks such as numerical calculation and text translation. Furthermore, in most cases, VaLiD surpasses other methods (VCD [20], M3ID [10], and Ritual [42]), highlighting its superior ability to reduce hallucinations and improve the reliability of the generated outputs.

### C. VaLiD is More Compatible than VCD

**Proof 1** Let  $\mathbb{P}_{valid} \circ \mathbb{P}_{vcd}$  and  $\mathbb{P}_{vcd} \circ \mathbb{P}_{valid}$  represent the application of VCD and VaLiD in different sequences. Considering that  $\mathbb{P}$  indicate an operator formed as  $(1 + \alpha)P_{ori} - \alpha P_{ref}$ , where  $\alpha$  and  $\alpha'$  are two positive coefficients to control the contrast intensity for VCD and VaLiD, respectively. Assuming truncation effects are negligible, then we have

$$\begin{aligned}
 \mathbb{P}_{valid} \cdot \mathbb{P}_{vcd}(P_{ori}) &= \mathbb{P}_{valid} [(1 + \alpha)P_{ori} - \alpha P_{noi}] \\
 &= (1 + \alpha') \cdot (1 + \alpha)P_{ori} - \alpha' P_{noi} - \alpha' P_{ent} \\
 &= (1 + \alpha')(1 + \alpha)P_{ori} - [\alpha(1 + \alpha')P_{noi} + \alpha' P_{ent}] \\
 \mathbb{P}_{vcd} \cdot \mathbb{P}_{valid}(P_{ori}) &= \mathbb{P}_{vcd} [(1 + \alpha')P_{ori} - \alpha' P_{ent}] \\
 &= (1 + \alpha) [(1 + \alpha')P_{ori} - \alpha' P_{ent}] - \alpha \cdot P_{noi} \\
 &= (1 + \alpha)(1 + \alpha')P_{ori} - [(1 + \alpha)\alpha' P_{ent} + \alpha P_{noi}] \\
 \|\mathbb{P}_{valid} \cdot \mathbb{P}_{vcd} - \mathbb{P}_{vcd} \cdot \mathbb{P}_{valid}\| & \\
 &= | - [\alpha(1 + \alpha')P_{noi} + \alpha' P_{ent}] + [(1 + \alpha)\alpha' P_{ent} + \alpha P_{noi}] | \\
 &= |\alpha' P_{ent} + \alpha\alpha' P_{ent} + \alpha P_{noi} - \alpha P_{noi} - \alpha\alpha' P_{noi} - \alpha' P_{ent}| \\
 &= \alpha\alpha' |P_{ent} - P_{noi}| \\
 &= \mathcal{K} |P_{ent} - P_{noi}|
 \end{aligned}$$

where  $P_{ori}$ ,  $P_{noi}$  and  $P_{ent}$  denote the original distribution, the reference distribution constructed by VCD, and the reference distribution constructed by VaLiD, respectively.  $\mathcal{K}$  denotes a constant value, determined by  $\alpha$  and  $\alpha'$ .

The results show that the order in which VCD and VaLiD are applied affects the model’s performance, with the difference in outcomes being proportional to the way each method constructs the reference distribution. Combining the experimental results from the Table 4, we observe that applying VCD first, followed by VaLiD, leads to further performance improvements. This reinforces the importance of addressing distortions in the visual encoding process as a critical factor in mitigating model hallucinations.

### D. More Case Studies

We provide more case studies on all benchmarks (POPE [24], AMBER [39]) to verify the efficacy of VaLiD in generative task. Results are shown in Figure 6.

Dataset	Setup	Method	Acc.↑	Precision	Recall	F1↑	Yes
MSCOCO [25]	Random	Vanilla	82.33	89.50	73.27	80.57	40.93
		VCD [20]	87.23	93.87	79.67	86.19	42.43
		M3ID [10]	86.53	94.70	77.40	85.18	40.87
		Ritual [42]	85.80	97.44	73.53	83.81	37.73
		VaLiD	88.60	95.45	81.06	87.67	42.47
	Popular	Vanilla	81.10	86.94	73.20	79.48	42.10
		VCD [20]	85.80	90.32	80.20	84.96	44.40
		M3ID [10]	84.63	90.75	77.13	83.39	42.50
		Ritual [42]	84.93	94.11	74.53	83.18	39.60
		VaLiD	85.89	91.74	80.73	85.89	44.00
	Adversarial	Vanilla	78.63	81.06	74.73	77.76	46.10
		VCD [20]	81.40	83.36	78.47	80.84	47.07
		M3ID [10]	81.70	84.99	77.00	80.80	45.30
		Ritual [42]	82.60	89.00	74.40	81.05	41.80
		VaLiD	83.67	84.64	82.27	83.43	48.60
A-OKVQA [36]	Random	Vanilla	85.53	87.69	82.67	85.11	47.13
		VCD [20]	87.90	88.26	87.20	87.72	49.40
		M3ID [10]	87.27	89.70	84.20	86.86	46.93
		Ritual [42]	89.27	93.69	84.20	88.69	44.93
		VaLiD	89.93	90.58	89.13	89.85	49.20
	Popular	Vanilla	81.43	81.92	80.67	81.29	49.23
		VCD [20]	82.47	80.44	85.80	83.03	53.33
		M3ID [10]	83.53	83.76	83.20	83.48	49.67
		Ritual [42]	86.60	87.81	85.00	86.38	48.40
		VaLiD	86.03	83.84	89.27	86.47	53.23
	Adversarial	Vanilla	75.47	72.82	81.27	76.81	55.80
		VCD [20]	76.60	72.41	85.93	78.60	59.33
		M3ID [10]	76.97	73.50	84.33	78.55	57.37
		Ritual [42]	79.07	77.08	82.73	79.81	53.67
		VaLiD	79.13	74.04	89.73	81.13	60.60
GQA [17]	Random	Vanilla	84.70	88.19	80.13	83.97	45.43
		VCD [20]	87.90	89.40	86.00	87.67	48.10
		M3ID [10]	86.20	88.90	82.73	85.70	46.53
		Ritual [42]	87.93	93.24	81.80	87.14	43.87
		VaLiD	88.70	89.20	88.07	88.63	49.37
	Popular	Vanilla	77.83	76.85	79.67	78.23	51.83
		VCD [20]	80.07	77.10	85.53	81.10	55.47
		M3ID [10]	78.60	77.97	79.73	78.84	51.13
		Ritual [42]	82.08	83.65	81.53	82.58	48.73
		VaLiD	82.20	79.27	87.20	83.05	55.00
	Adversarial	Vanilla	75.70	73.93	79.40	76.57	53.70
		VCD [20]	76.30	72.63	84.40	78.08	58.10
		M3ID [10]	77.20	75.19	81.20	78.08	54.00
		Ritual [42]	80.10	79.00	82.00	80.47	51.90
		VaLiD	78.83	74.59	87.47	80.52	58.63

Table 5. Results of LLaVA-v1.5 on POPE benchmark.

Dataset	Setup	Method	Acc.↑	Precision	Recall	F1↑	Yes
MSCOCO [25]	Random	Vanilla	82.20	83.45	80.33	81.86	48.13
		VCD [20]	84.37	86.95	80.87	83.80	46.50
		M3ID [10]	79.77	83.20	74.60	78.66	44.83
		Ritual [42]	85.33	93.80	75.67	83.76	40.33
		VaLiD	85.93	94.04	76.73	84.51	40.80
	Popular	Vanilla	79.10	78.55	80.07	79.30	50.97
		VCD [20]	81.23	82.24	79.67	80.93	48.43
		M3ID [10]	76.80	77.80	75.00	76.37	48.20
		Ritual [42]	82.87	88.40	75.67	81.53	42.80
		VaLiD	83.40	88.90	76.33	82.14	43.93
	Adversarial	Vanilla	76.87	75.25	80.07	77.58	53.20
		VCD [20]	78.53	78.12	79.27	78.69	50.73
		M3ID [10]	74.93	73.79	77.33	75.52	52.40
		Ritual [42]	80.77	84.26	75.67	79.73	44.90
		VaLiD	81.43	84.64	76.80	80.53	45.36
A-OKVQA [36]	Random	Vanilla	80.50	77.54	85.87	81.49	55.37
		VCD [20]	83.13	80.79	86.93	83.75	53.80
		M3ID [10]	78.53	79.00	77.73	78.36	49.20
		Ritual [42]	84.53	88.31	79.60	83.73	45.07
		VaLiD	87.00	88.12	85.53	86.81	48.53
	Popular	Vanilla	76.57	72.55	85.47	78.48	58.90
		VCD [20]	78.76	74.76	86.87	80.36	58.10
		M3ID [10]	76.67	75.74	78.47	77.08	51.80
		Ritual [42]	81.83	83.14	79.87	81.47	48.03
		VaLiD	82.90	79.92	85.20	82.48	53.30
	Adversarial	Vanilla	70.43	65.66	85.67	74.34	65.23
		VCD [20]	72.83	67.96	86.40	76.08	63.57
		M3ID [10]	68.23	65.15	78.40	71.16	60.17
		Ritual [42]	74.63	72.49	79.40	75.79	54.77
		VaLiD	75.60	71.40	85.40	77.78	59.80
GQA [17]	Random	Vanilla	79.17	75.72	85.86	80.47	56.70
		VCD [20]	82.10	79.85	85.87	82.75	53.77
		M3ID [10]	78.37	79.08	77.13	78.10	48.77
		Ritual [42]	83.26	87.69	77.40	82.23	44.13
		VaLiD	85.20	86.62	83.27	84.91	48.07
	Popular	Vanilla	74.23	69.98	84.87	76.71	60.63
		VCD [20]	76.63	72.51	85.80	78.60	59.17
		M3ID [10]	74.07	72.53	77.47	74.92	53.40
		Ritual [42]	79.33	79.45	79.13	79.29	49.80
		VaLiD	78.37	75.77	83.40	79.40	55.03
	Adversarial	Vanilla	71.13	66.49	85.20	74.69	64.07
		VCD [20]	73.27	68.10	87.53	76.60	64.27
		M3ID [10]	68.80	66.26	76.60	71.06	57.80
		Ritual [42]	74.67	72.64	79.13	75.75	54.47
		VaLiD	75.23	71.89	82.87	76.99	57.63

Table 6. Results of InstructBLIP on POPE benchmark.

Dataset	Setup	Method	Acc.↑	Precision	Recall	F1↑	Yes
MSCOCO [25]	Random	Vanilla	85.17	96.56	72.93	83.10	37.77
		VCD [20]	87.17	97.13	76.60	85.65	39.43
		M3ID [10]	85.97	97.79	73.60	83.99	37.63
		Ritual [42]	85.40	98.90	71.60	83.06	36.20
		VaLiD	88.10	96.96	78.67	86.86	40.57
	Popular	Vanilla	84.73	95.38	73.00	82.70	38.27
		VCD [20]	86.07	94.64	76.47	84.59	40.40
		M3ID [10]	84.87	95.40	73.27	82.88	38.40
		Ritual [42]	84.84	97.20	71.73	82.55	36.90
		VaLiD	87.13	94.28	79.07	86.00	41.93
	Adversarial	Vanilla	83.33	90.92	74.07	81.63	40.73
		VCD [20]	84.27	90.28	76.80	83.00	42.53
		M3ID [10]	83.23	91.16	73.60	81.45	40.37
		Ritual [42]	82.80	93.16	70.80	80.45	38.00
		VaLiD	84.43	88.57	79.07	83.55	44.63
A-OKVQA [36]	Random	Vanilla	86.80	94.30	78.33	85.58	41.53
		VCD [20]	87.80	94.23	80.53	86.84	42.73
		M3ID [10]	87.43	95.54	78.53	86.21	41.10
		Ritual [42]	86.10	96.09	75.27	84.41	39.16
		VaLiD	88.70	93.55	83.13	88.03	44.43
	Popular	Vanilla	86.73	95.16	77.40	85.37	40.67
		VCD [20]	87.53	93.17	81.00	86.66	43.47
		M3ID [10]	87.27	94.86	78.80	86.09	41.53
		Ritual [42]	85.77	95.97	74.67	83.99	38.90
		VaLiD	88.90	93.19	83.93	88.32	45.03
	Adversarial	Vanilla	80.87	83.21	77.33	80.17	46.47
		VCD [20]	81.80	82.54	80.67	81.59	48.87
		M3ID [10]	81.40	83.50	78.27	80.80	46.87
		Ritual [42]	80.83	84.85	75.07	79.66	44.23
		VaLiD	82.26	81.59	83.33	82.45	51.07
GQA [17]	Random	Vanilla	84.40	89.75	77.67	83.27	43.27
		VCD [20]	86.73	91.43	81.07	85.94	44.33
		M3ID [10]	85.93	91.40	79.33	84.94	43.40
		Ritual [42]	85.80	93.52	76.93	84.42	41.13
		VaLiD	89.97	94.31	85.07	89.45	45.10
	Popular	Vanilla	80.50	82.02	78.13	80.03	47.63
		VCD [20]	82.33	83.22	81.00	82.09	48.67
		M3ID [10]	81.07	83.72	77.13	80.29	46.07
		Ritual [42]	82.56	87.84	75.60	81.26	43.03
		VaLiD	84.40	84.13	84.80	84.46	50.40
	Adversarial	Vanilla	79.33	79.81	78.53	79.17	49.20
		VCD [20]	81.10	81.08	81.13	81.11	50.03
		M3ID [10]	79.83	80.50	78.73	79.61	48.90
		Ritual [42]	80.33	83.65	75.40	79.31	45.06
		VaLiD	82.33	80.89	84.67	82.74	52.33

Table 7. Results of Qwen-VL on POPE benchmark.

Model	Method	Perception										Cognition			
		existence	count	position	color	posters	celebrity	scene	landmark	artwork	OCR	commonsense reasoning	numerical calculation	text translation	code reasoning
LLaVA-v1.5	Vanilla	185.00	143.33	<b>128.33</b>	143.33	113.95	109.12	151.25	134.75	113.75	115.00	100.71	62.50	75.00	80.00
	VCD [20]	185.00	142.67	118.33	158.33	130.95	<b>124.71</b>	149.75	138.00	109.75	110.00	116.43	87.50	47.50	70.00
	M3ID [10]	185.00	130.00	118.33	145.00	126.53	124.12	147.00	141.75	108.00	110.00	107.14	52.50	82.50	<b>95.00</b>
	Ritual [42]	<b>190.00</b>	138.33	118.33	<b>160.00</b>	<b>141.50</b>	116.18	<b>158.50</b>	<b>150.00</b>	<b>120.75</b>	115.00	<b>116.43</b>	42.50	<b>87.50</b>	85.00
	VaLiD	<b>190.00</b>	<b>147.33</b>	125.00	<b>160.00</b>	<b>143.54</b>	<b>129.41</b>	<b>154.50</b>	<b>145.00</b>	<b>115.00</b>	<b>127.50</b>	<b>115.71</b>	<b>70.00</b>	60.00	62.50
InstructBLIP	Vanilla	170.00	78.33	65.00	106.67	114.63	110.88	138.50	120.50	86.00	67.50	87.86	<b>90.00</b>	72.50	77.50
	VCD [20]	180.00	<b>88.33</b>	<b>75.00</b>	<b>136.67</b>	120.41	120.00	150.00	138.75	96.00	80.00	97.14	60.00	62.50	47.50
	M3ID [10]	175.00	80.00	76.67	105.00	131.29	113.23	149.00	118.75	100.75	70.00	<b>114.29</b>	67.50	77.50	70.00
	Ritual [42]	<b>180.00</b>	68.33	68.33	120.00	<b>133.33</b>	<b>152.65</b>	<b>161.25</b>	<b>149.25</b>	<b>104.75</b>	<b>140.00</b>	113.57	72.50	<b>82.50</b>	60.00
	VaLiD	<b>185.00</b>	<b>83.33</b>	<b>78.33</b>	<b>145.00</b>	<b>121.77</b>	<b>135.88</b>	<b>153.75</b>	<b>154.00</b>	<b>109.75</b>	<b>95.00</b>	<b>106.43</b>	50.00	<b>95.00</b>	<b>77.50</b>
Qwen-VL	Vanilla	175.00	131.67	141.67	165.00	<b>174.15</b>	147.65	152.75	150.25	128.50	122.50	104.29	27.50	105.00	57.50
	VCD [20]	170.00	131.67	151.67	175.00	167.35	<b>156.47</b>	153.50	153.50	<b>143.00</b>	110.00	<b>112.14</b>	35.00	112.50	47.50
	M3ID [10]	<b>180.00</b>	<b>141.67</b>	145.00	180.00	168.37	152.35	151.50	157.50	131.75	125.00	101.43	42.50	107.50	<b>67.50</b>
	Ritual [42]	170.00	128.33	<b>168.33</b>	<b>180.00</b>	171.43	149.12	<b>154.25</b>	<b>169.25</b>	138.75	<b>130.00</b>	104.29	<b>60.00</b>	<b>140.00</b>	57.50
	VaLiD	<b>185.00</b>	<b>155.00</b>	<b>148.33</b>	<b>185.00</b>	170.41	<b>152.94</b>	<b>162.00</b>	<b>167.00</b>	<b>138.00</b>	80.00	<b>127.86</b>	<b>42.50</b>	<b>145.00</b>	<b>75.00</b>

Table 8. Numerical results of MME benchmark. The table presents the MME scores of various models across multiple perception and cognition tasks. The best performances and second best performances within each setting are **bolded**.



**VaLiD:** The image depicts three dogs running together in a large, lush green field. They appear to be enjoying a game of fetch or simply having fun running around. One dog is located on the left side of the field, another in the middle, and the third one is towards the right side. A sports ball can be seen in the middle of the field, capturing the dogs' attention as they run towards it. The scene evokes a sense of joy and energy, showcasing the dogs' playful nature and the beauty of the open, grassy field.

**Vanilla:** The image features **two** dogs playing together in a grassy field. One dog is closer to the left side of the field, while the other dog is positioned more towards the right side. They are both chasing a yellow ball, which is located in the middle of the field. The dogs are enjoying their playtime, running and jumping around the field.

**VaLiD:** The image depicts a peaceful scene of two giraffes walking and standing together in a grassy field. They are positioned close to each other, possibly enjoying each other's company or searching for food. The grassy field is surrounded by trees, creating a natural habitat for the giraffes. A third giraffe is visible in the distance, further back in the field. The overall atmosphere of the image conveys a sense of tranquility and harmony within the wildlife environment.



**Vanilla:** The image features a group of **four** giraffes standing in a grassy field. They are spread out across the scene, with one giraffe on the left side, another in the middle, **and two more on the right side**. The giraffes are positioned near a tree, which can be seen in the background. The scene is set in a lush green field, providing a natural habitat for the giraffes.



**VaLiD:** In the image, a man is standing on a grassy field, playing with his dog by throwing a red frisbee for it to chase and catch. The dog is actively running towards the frisbee, displaying its agility and enthusiasm for the game. The man and dog appear to be the main focus of the scene, likely enjoying their time outdoors. In addition, several cars can also be seen parked in the distance, indicating that this location might be a park or recreational area.

**Vanilla:** In the image, a man is standing in a grassy field, holding a red frisbee. A dog is nearby, eagerly waiting for the frisbee to be thrown. The man appears to be preparing to throw the frisbee, while the dog is ready to catch it. The scene captures a fun and active moment between the man and his dog. In addition, **there are several people nearby**.

**VaLiD:** The scene features a rustic truck driving down a dirt road, carrying several passengers on its back. There are three people visible in the truck, with one person sitting on the left side of the truck and two others riding on the back. In addition to the passengers on the truck, there is another person on a motorcycle following behind it, slightly to the right. A suitcase can also be spotted near the center of the image, possibly belonging to one of the passengers or the motorcyclist. The overall atmosphere suggests a journey through a rural or remote area.



**Vanilla:** The image features a small truck driving down a dirt road, **with a man and a woman riding in the back**. The truck is carrying a large amount of luggage, including suitcases and a backpack. The passengers appear to be enjoying their journey, as they are both smiling. In addition to the truck, there is a motorcycle parked on the side of the road, **and a bicycle is visible further down the road**. The scene suggests a casual, leisurely trip for the passengers, possibly exploring the countryside or traveling to a nearby destination.

Figure 6. Illustration of hallucination correction by our proposed VaLiD with four more cases from AMBER [39] and POPE [25] dataset. Hallucinated objects from vanilla decoding are highlighted in **red**.